Available online at www.sciencedirect.com

SCIENCE DIRECT

Biochimica et Biophysica Acta 1690 (2004) 33–41

BIOCHIMICA ET BIOPHYSICA ACTA BBA

www.bba-direct.com

Ultrastructural organization of ex vivo amyloid fibrils formed by the apolipoprotein A-I Leu174Ser variant: an atomic force microscopy study

Annalisa Relini[a,*], Ranieri Rolandi[a], Martino Bolognesi[a,b], Manuela Aboudan[c,d], Giampaolo Merlini[c,d], Vittorio Bellotti[c,d], Alessandra Gliozzi[a]

[a] *National Institute for the Physics of Matter and Department of Physics, University of Genoa, via Dodecaneso 33, I-16146, Genoa, Italy*
[b] *Center for Excellence in Biomedical Research, Genoa, Italy*
[c] *Department of Biochemistry, University of Pavia, Italy*
[d] *Laboratory of Biotechnology, IRCCS Policlinico S. Matteo, Italy*

Received 21 January 2004; received in revised form 20 April 2004; accepted 21 April 2004
Available online 26 May 2004

Abstract

Atomic force microscopy was employed to study ex vivo amyloid material isolated from the transplanted hearts of two patients affected by systemic amyloidosis caused by the Leu174Ser apolipoprotein A-I variant. The purified material consists of fibrils and globular aggregates. For both patients the same morphological patterns are observed; in addition, fibril diameters obtained for the two patients turn out to be compatible, both in air (2.00 ± 0.02 and 2.04 ± 0.04 nm) and under liquid (10.7 ± 0.4 and 11.3 ± 0.5 nm). Fibrils display heterogeneous morphologies, occasionally showing a left-handed twist. Inspection of fibril ends, the study of fibril contour shape and the analysis of partially unfolded fibrils yield independent evidences suggesting that most twisted fibrils are composed of three protofilaments. The size of globular aggregates is the same for both patients (4.4 ± 0.4 and 5.1 ± 0.5 nm, measured under liquid) and is compatible with the protofilament expected diameter, suggesting that globules may represent protofilament precursors.

Keywords: Amyloid; Apolipoprotein A-I; Atomic force microscopy

1. Introduction

The intracellular and extracellular deposition of protein aggregates having a fibrillar conformation is often considered as the hallmark of several fatal diseases, such as Alzheimer's disease, Parkinson's disease, Spongiform encephalopathy, Huntington Corea and Amyloidosis [1]. It has been proposed that the pathogenic mechanism common to these diseases is the polymerisation of monomeric protein precursors [2]. The conversion of protein monomers into fibrillar polymers is a multiple-phase process which occurs through formation of intermediate products. Indeed, one of the main goals of structural biology studies in this field is the detailed characterisation of all the intermediates involved in the fibril formation process.

Many efforts have been so far devoted to determining the three dimensional structure of protein monomers, oligomers, protofilaments and fibrils [3]. Whereas substantial information is available on the three dimensional structure of the monomeric precursors, much more limited data are available for the oligomeric pre-fibrillar aggregates that transiently appear in the fibril formation process, and on the polypeptide conformation achieved within the fibril scaffold. Information on the ultrastructural organization of fibrils has been recently provided through the analysis of fibrils formed by amyloidogenic proteins such as Aβ protein [4,5], calcitonin [6], ApoSAA [7], amylin [8], PrPSc [9], SH3 domain [10], immunoglobulin light chains [11], β2-microglobulin [12], transthyretin [13], lysozyme [14], apolipoprotein A-I [14] and C-II [15].

The atomic force microscope (AFM) is a unique tool for studying the structure of amyloid protofilaments and fibrils [16], since it combines the ultrastructural analysis of the sample surface with the capability of imaging the specimens

* Corresponding author. Tel.: +39-10-3536427; fax: +39-10-314218.
E-mail address: relini@fisica.unige.it (A. Relini).

0925-4439/$ - see front matter © 2004 Elsevier B.V. All rights reserved.
doi:10.1016/j.bbadis.2004.04.007

under physiological fluid environment. The number of cases in which AFM has been used in the analysis of in vitro fibrils is highly dominant over the analysis of ex vivo specimens, likely due to difficulties related to the recovery of natural samples. However, analyses of fibrils extracted from ex vivo pathological deposits are fundamental for comparative studies with fibrils assembled in vitro, on one hand, and with the histological specimens where fibrils are not removed from their biological environment, on the other.

Here we report an AFM analysis of natural amyloid fibrils produced by the Leu174Ser apolipoprotein A-I variant (apoA-I-LS). ApoA-I is the primary protein constituent of high density lipoprotein (HDL) particles, responsible for cholesterol extraction and transport from body tissues. Variant forms of ApoA-I are involved in some forms of hereditary systemic amyloidosis. The fibrils examined in this study are associated with a familial form of systemic amyloidosis with predominant heart involvement and were isolated from the heart of two patients heterozygous for the mutation. As far as we know, amyloid fibrils resulting from aggregation of apoA-I have not been analysed before by AFM. The ultrastructural information available so far is based on small angle X-ray diffraction of the apoA-I-LS mutant [17], and on electron microscopy cross-sectional images of natural fibrils of the Leu60Arg apoA-I mutant [18]. Characterization of the ultrastructural assembly of ApoA-I-LS in natural amyloid fibrils can provide complementary information on the three-dimensional organization of this type of fibrillar deposits. In this work we compare the morphologies observed in ApoA-I-LS amyloid material obtained from two different patients, determining the structural parameters of the aggregates observed both in air and under liquid. In addition, we discuss the role of the non-fibrillar aggregates, coexisting with the fibrils, as potential fibril precursors.

There are increasing evidences that amyloid can be considered as a generic structural state of proteins. The relevance of studies in this field stretches beyond the specificity of the system examined, contributing to the growing host of data collected to reach a deeper understanding of this intriguing process.

2. Materials and methods

2.1. Preparation and purification of apoA-I-LS

Fibrils were isolated from the explanted hearts of two patients presenting cardiac amyloidosis caused by the apolipoprotein variant Leu174Ser [17,19]. Amyloid material was purified by the water extraction procedure according to the Pras method [20] with minor modifications. Approximately 800 mg of tissue was repeatedly homogenised and centrifuged at 60,000 × *g* in 2 ml of buffer containing 10 mM Tris, 1 mM EDTA, 140 mM NaCl, 1.5 mM phenylmethylsulfonyl fluoride ($PhMeSO_2F$) and 0.1% NaN_3, pH 8.0. The procedure that allowed the clearing of the non-amyloid material was stopped when the absorbance at 280 nm of the supernatant dropped under 0.1 units. At that point the buffer was replaced by distilled water, and homogenization and centrifugation was carried out six times. Amyloid fibrils were recovered in the supernatant and their concentration monitored by Congo red staining and thioflavin assay [21]. For AFM studies, fractions IV and V of the H_2O extraction, containing the highest amyloid amount, were preferentially used.

The characterization of the main protein constituent of these fibrils was performed as previously described by a combination of amino acid sequence and mass spectrometry [17,22]. Aliquots of the water extraction fraction IV and V were analysed for protein content by Coomassie brilliant blue G-259 protein assay (Bio Rad); a volume of fibrils solution containing 1 mg of protein was lyophilised and extracted with chloroform and methanol (2:1, v/v). The fatty acid methyl esters (FAMEs) were prepared from lipids according to the procedure described by Watkins et al. [23] and their identification and quantitation was carried out through a gas chromatography/mass spectrometry system (Agilent Technology 5973N/6890N.). FAMEs standards were provided by SIGMA.

2.2. Atomic force microscopy

For AFM inspection, the amyloid material was diluted to the concentration of 50 μg/ml in Tris 50 mM, pH 7 and a small aliquot (20 μl) was deposited on freshly cleaved mica. For imaging in air, the sample was dried under mild vacuum for 30 min; for imaging in liquid, the sample was incubated on mica for 30 min and then rinsed with the same buffer to eliminate the material which had not adhered to the substrate.

AFM images were acquired in tapping mode in a vibration insulated environment, using a Dimension 3000 microscope (Digital Instruments), software version 4.42r4, equipped with a 'G' scanning head (maximum scan size 100 μm). For imaging in liquid, we used V-shaped gold-coated Si_3N_4 cantilevers (200-μm length, nominal spring constant 0.06 N/m) with pyramidal tips having nominal curvature radii of about 40 nm; for imaging in air, we used single beam uncoated silicon cantilevers (type OMCL-AC160TS-W, Olympus). The drive frequency was around 6 kHz in liquid and 300 kHz in air; the scan rate was between 0.3 and 0.5 Hz.

The curvature radii of the tips were determined by imaging dried calibration latex spheres [24] 94 nm in diameter. The sample was obtained by drying a drop of latex sphere suspension on a mica surface.

The horizontal displacements of the piezoelectric tube were calibrated using a 10-μm pitch diffraction grating; vertical displacements were calibrated measuring the depth of grating notches (180 nm) and the half unit cell steps (1

nm) obtained by treating freshly cleaved mica with hydrofluoric acid.

3. Results

The ApoA-I-LS amyloid fibrils, extracted from cardiac amyloid deposits, are extraordinarily homogeneous in composition in both cases, displaying a single molecular component of 10,724 Da, corresponding to the 1–93 peptide of wild-type apoA-I. The fibrils from both patients give rise to identical small angle X-ray diffraction patterns, indicative of residual coiled coil α-helical structure conformation [17]. The homogeneity of the amyloidogenic polypeptide isolated in the two cases may be due to the peculiar source of this material, derived from hearts explanted during transplantation procedures, such that the protein was presumably not exposed to the degradative processes which may occur in autoptic biological samples. The polypeptide 1–93, otherwise, can be considered highly representative of the main apoA-I amyloid fibrils component in man. In fact, as recently reviewed by Andreola et al. [22], independently of the site and type of the amyloidogenic mutation, all chemically characterized fibrils display the 1–93 polypeptide as one of the most abundant components. The chemical analysis of these natural fibrils also included the identification and quantitation of fatty acids possibly associated with the amyloidogenic lipoprotein. We have calculated that 1 mg of fibrillar protein approximately contains 26 μg of linoleic acid, 11 μg of palmitic acid and 9 μg of oleic acid. Other fatty acids were detectable in traces. A weight/weight ratio of protein/lipid in these fibrils is therefore approximately 50:1.

Tapping mode AFM has been employed to obtain detailed topographical information on the apoA-I-LS fibril structure, performing measurements both in liquid environment and in air. All the materials examined are the result of aqueous extraction procedures; none of the samples was treated with chaotropic agents or organic solvents, nor was submitted to lyophilization.

3.1. Measurements in air

When the fibrillar material is dried on mica, three different typical patterns, often coexisting in different regions of the same sample, are detected by AFM analysis. In the first pattern many fibrils, in the length range between 0.2 and 1.5 μm, are scattered on a background composed of closely packed material of globular shape (Fig. 1). The second typical pattern observed consists of fibrils radially diverging from a spherulite, with the bare mica substrate visible in the background (Fig. 2). In this case no globular material is generally observed. The third pattern is represented by very dense aggregates of closely packed fibrils or fibril fragments (Fig. 3). Fibril width and height are conveniently measured in isolated, individual

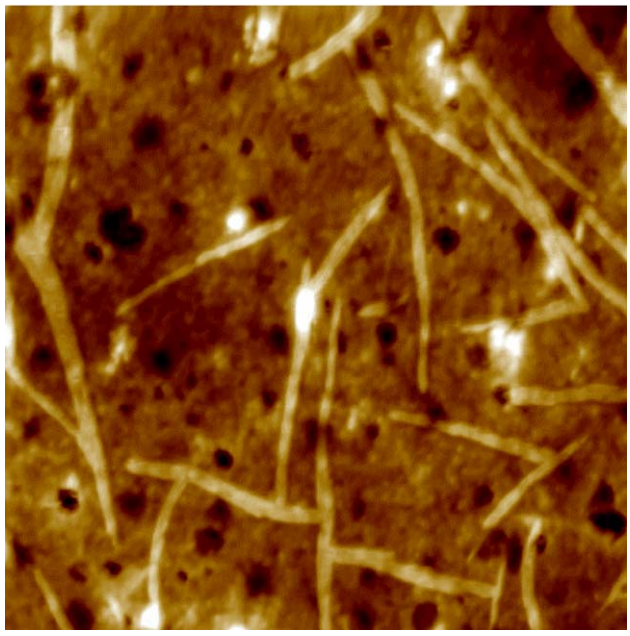

Fig. 1. Tapping mode AFM image (height data, obtained in air) of Leu174Ser apo A-I amyloid material dried on mica, revealing fibrils on a background of globular material. The dark regions in the background are places where the globular material is absent and the bare mica is visible. Scan size, 1.5 μm; *Z* range, 20 nm (For color see online version).

fibrils from the image sections taken perpendicularly to the fibril longitudinal axis. The fibril width is broadened by "tip convolution" effects, which, however, do not affect the fibril maximum height. Accordingly, the distributions of fibril diameters shown in this paper were obtained measuring the height in cross section of the fibrils.

Fig. 4 compares the distributions of fibril diameters for patients A and B, resulting, respectively, from 306 and 365 height measurements. Each distribution was obtained from different samples, imaged at different times. The mean values of the distributions are 2.00 ± 0.02 nm for patient A and 2.04 ± 0.04 nm for patient B, i.e. values perfectly comparable within the experimental error. For both patients, the fibril height does not show a unimodal distribution, indicating coexistence of more than one fibril population of different size. However, since within single experimental runs, with a number of measurements per run which ranged from 30 to 270, we obtained unimodal distributions, it is likely that the different populations result from different fibril swelling, as a consequence of varying environmental humidity conditions in the independent measurements.

The observed fibril morphology turns out to be quite heterogeneous, especially in the case of scattered fibrils (pattern 1). Most fibrils generally appear as flat ribbons or cylinders without revealing details of their structure. Some fibrils, however, clearly show a twisted structure (Fig. 5), with a helical periodicity in the 60–80-nm range, measured as the horizontal distance between two

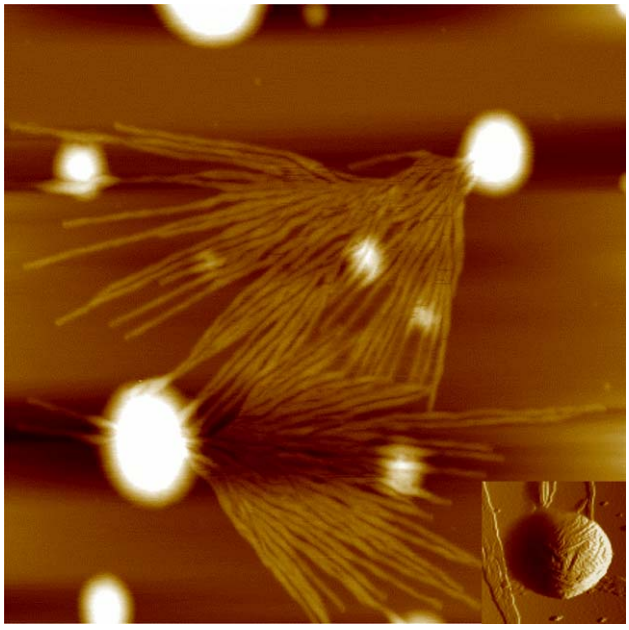

Fig. 2. Tapping mode AFM image (height data, obtained in air) of Leu174Ser apo A-I amyloid material dried on mica, showing bundles of fibrils diverging from spherulites. Since the height of the spherulites is much larger than the single fibril size, they appear white in the height image. Amplitude data, reported in the inset, show that these spherulites are made of a tight winding of fibrils. Scan size, 1.27 μm; *Z*, range 20 nm (For color see online version).

adjacent maxima in the longitudinal profile of the fibril. The fibril twist is usually observed as left-handed, in agreement with previous observations on amyloid fibrils [12,16].

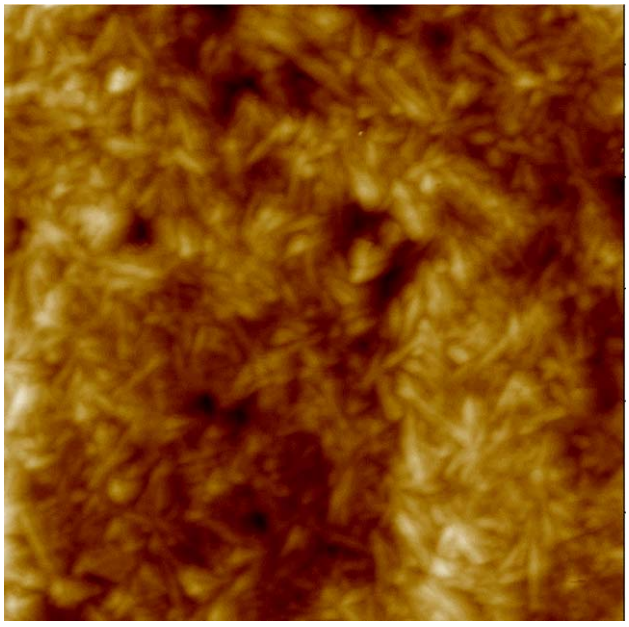

Fig. 3. Tapping mode AFM image (height data, obtained in air) of Leu174Ser apo A-I amyloid material dried on mica, showing a region of densely packed fibrils and fibril fragments. Scan size, 1.38 μm; *Z* range, 40 nm (For color see online version).

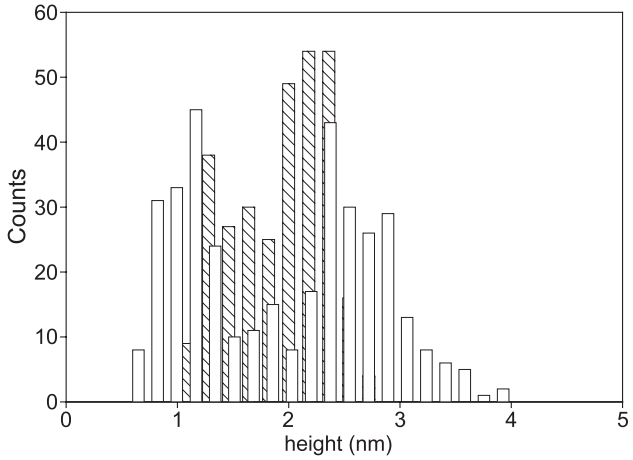

Fig. 4. Histogram of fibril diameters, obtained measuring the height of fibril cross sections in the AFM images in air. The different populations correspond to patient A (dashed) and patient B (white) and result from 306 and 365 measurements, respectively. The fibril diameters turn out to be 2.00 and 2.04 nm with standard errors of 0.02 and 0.04, respectively.

Further information on fibril structure can be obtained by studying the shape of the twisted fibrils. Perutz et al. [25], modelling fibrils with a bundle of plastic tubes, observed that the shape contour of the fibril changes according to the number of protofilaments composing the fibril. In fact, the way protofilaments overlap depends on their number: two filaments overlap symmetrically along the center of the fibril, three filaments overlap alternately

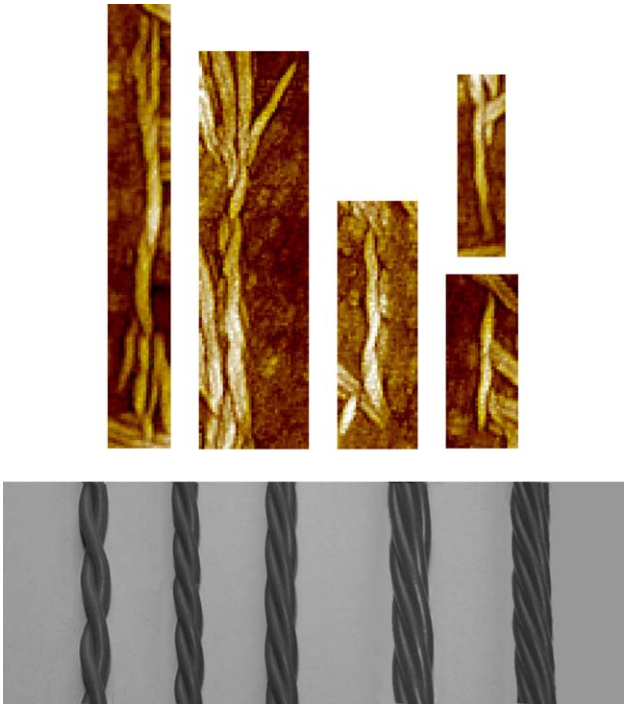

Fig. 5. Comparison between the shape contour of apo A-I twisted fibrils and models made of plastic tubes. From left to right, the models comprise fibrils made of two to six tubes (For color see online version).

on either side, while four overlap alternately on both sides and in the center, and so on, giving rise to distinguishable shape contours. Following this approach (Fig. 5), we compared the fibril shapes extracted from the AFM images with those expected for fibrils composed of two to six protofilaments. We found that fibrils composed of three intertwined protofilaments are the most common structures observed, although fibrils likely composed of four protofilaments are occasionally recognized. When several fibrils lie almost parallel and close to one another, one or more protofilaments unwinding from a fibril and winding onto an adjacent one are often observed. This phenomenon creates a sort of superstructure, interconnecting many parallel fibrils.

The number of protofilaments observed in the partially unwound fibril regions is always less than or equal to three (Fig. 6). An independent evidence supporting the idea that the fibril structures are mainly based on three protofilaments is provided by the analysis of fibril ends, which, in some cases, show different protofilament lengths. Therefore, a longitudinal section measured at the end of the fibril, as shown in Fig. 7, reveals a total of three discrete steps of the same height, corresponding, in this case, to a protofilament diameter of 0.74 nm.

3.2. Measurements under liquid

For samples imaged under liquid, a rather poor adhesion of fibrils to the mica substrate is observed. A typical pattern is shown in Fig. 8. The fibril length usually falls in the 250–500-nm range; longer fibrils were not able to adhere properly to the substrate. On the contrary, globular material is easily adsorbed on mica, being uniformly scattered in the background of the acquired images, and representing the majority of the structured matter observed. We measured the electrostatic repulsive force in solution by acquiring AFM force–distance curves, and found that under our experimental conditions practically no electrostatic repulsion is acting between tip and sample. Since it is known that the silicon nitride tip is negatively charged in solution [26], the above results suggest that the sample surface charge must be very low. Such indication is referred to the whole sample surface, being impossible to distinguish between the contributions arising from the globular structures and the fibrils. However, it is expected

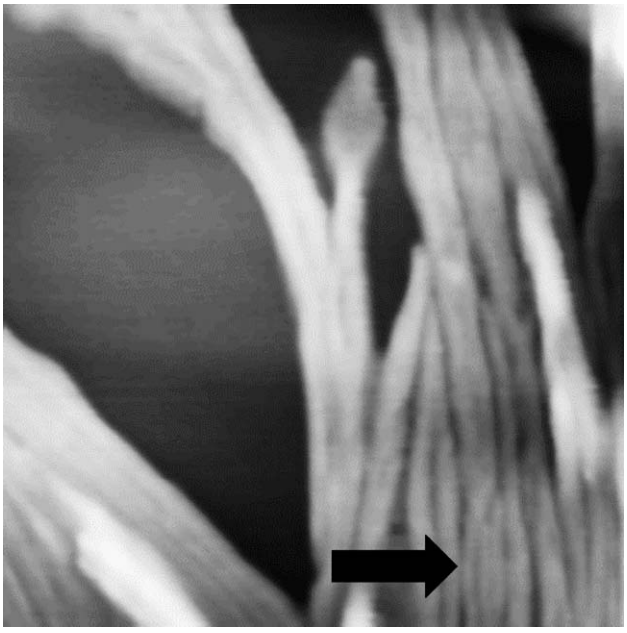

Fig. 6. Tapping mode AFM image (height data, obtained in air) of Leu174Ser apo A-I amyloid fibrils dried on mica. The black arrow indicates a region where the fibril is unwound, clearly showing three distinct protofilaments. Scan size, 500 nm; *Z* range, 15 nm.

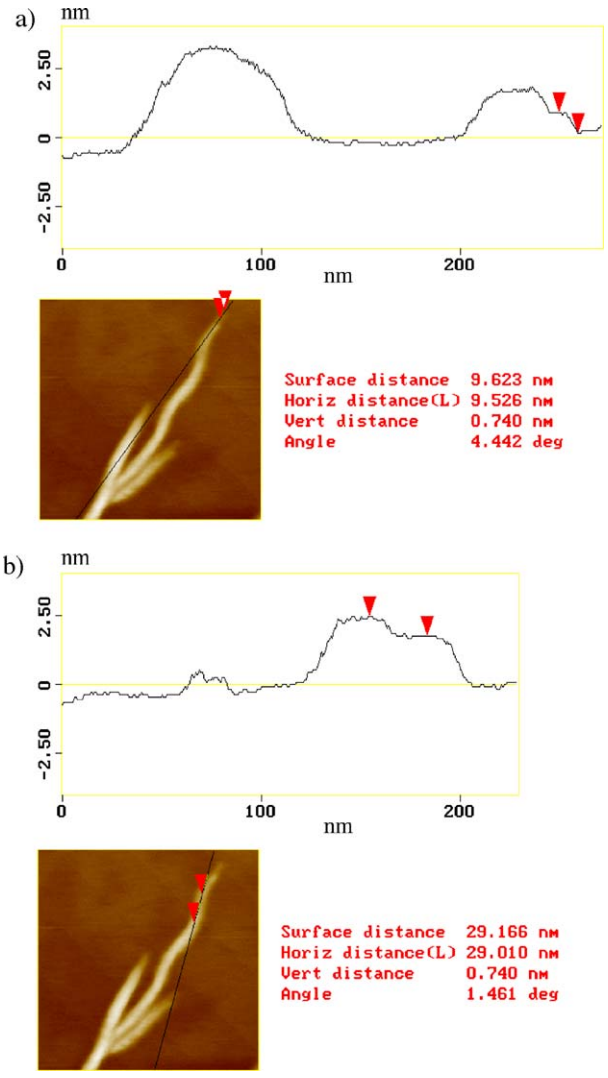

Fig. 7. Sections of the end of a fibril revealing the presence of steps of the same height. Since the fibril is not straight and the microscope software allows sectioning along straight lines only, it is necessary to section the fibril along two different directions to obtain the complete sequence of the steps. (a) section revealing two steps; (b) section revealing a third step of the same height as measured in (a) (For color see online version).

that positive charges compensating the negative surface charge of the mica substrate are displayed by at least one of these species. Specifically designed experiments will be required to establish whether a difference in the surface charge distribution between the globular material and the large fibrils is at the basis of the different substrate adhesion behaviour observed. Recently, it has been reported that apoC-II fibrils did not remain fixed to the mica substrate in the presence of buffer, while were attached to poly-L-lysine-coated mica [15]. This suggests that fibrils are negatively charged.

Measuring the height in cross section, we obtained unimodal distributions of fibril diameters in liquid environment for both patients (Fig. 8, inset). The fibril diameters are 10.7 ± 0.4 and 11.3 ± 0.5 nm for patients A and B, respectively. These values are identical, within experimental errors, and are significantly larger than those obtained in air. The absence of significant electrostatic repulsion between tip and sample under liquid should exclude the presence of artifacts, possibly resulting in an increase in the height of surface features [27]. The globules show height distributions with values of 4.4 ± 0.4 and 5.1 ± 0.5 nm for patients A and B, respectively. Within experimental errors, these values are coincident. As mentioned previously, globular material is also observed in air, but it is too closely packed to allow reliable height measurements. The

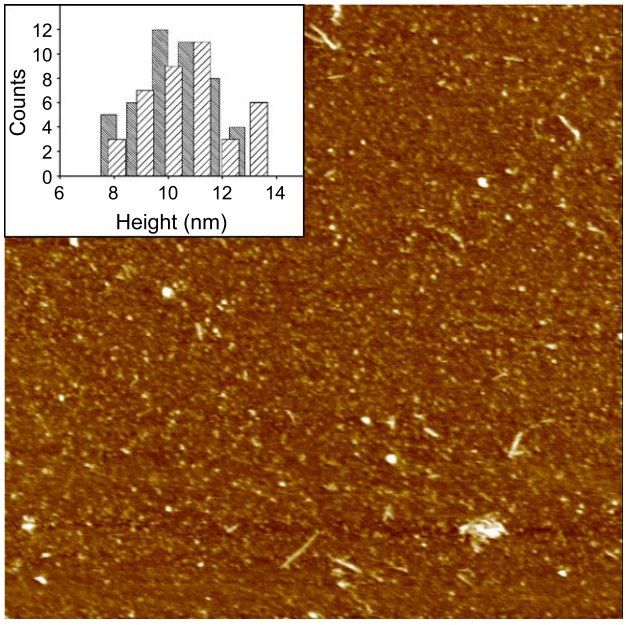

Fig. 8. Tapping mode AFM image (height data, obtained in liquid) of Leu174Ser apo A-I amyloid material, showing many globules and a few fibrils adhered on the mica surface. Scan size, 4.8 μm; *Z* range, 20 nm. Inset, histogram of fibril diameters, obtained measuring the height of fibril cross sections in the AFM images in liquid. The different populations correspond to patient A (fine dash) and patient B (coarse dash) and result from 46 and 39 measurements, respectively. The fibril diameters turn out to be 10.7 and 11.3 nm with standard errors of 0.4 and 0.5 nm, respectively (For color see online version).

Table 1
Structural data of Leu174Ser apo A-I amyloid material obtained by atomic force microscopy

Environment (nm)	Globule height (nm)	Protofilament diameter (nm)	Fibril height (nm)	Helical periodicity
Air	–	0.74	2.00 ± 0.02 (A) 2.04 ± 0.04 (B)	60–80
Aqueous	4.4 ± 0.4 (A) 5.1 ± 0.5 (B)	–	10.7 ± 0.4 (A) 11.3 ± 0.5 (B)	–

structural parameters obtained by the AFM analysis of the apoA-I-LS material are collected in Table 1.

4. Discussion

To check the actual shape of the fibril section, we have compared width and height measured from the image cross section. In principle, deposition of the fibril on a solid substrate might cause deformation of the fibril cross section. In addition, fibril width is expected to be broadened by tip convolution effects, which are predictable on the basis of simple geometrical models. When the height of the imaged object is smaller than the tip curvature radius, the tip can be modelled as a sphere. Assuming that the fibril sections are circular, the apparent width (w) is related to the height (h) according to the equation:

$$w = 4\sqrt{2Rh} \quad (1)$$

where R is the tip radius of curvature, h is the measured fibril height and w the predicted fibril width as a consequence of tip-induced broadening. For each cantilever employed in the experiments, the tip radius of curvature was determined as described in Section 2. In air, the measured fibril widths are significantly larger than the values predicted on the basis of Eq. (1), indicating that the drying procedure induces a flattening of the fibrils on the mica substrate. On the contrary, the fibril widths measured in liquid turn out to be in good agreement with the values predicted by Eq (1), indicating that, within experimental errors, no significant asymmetry of the fibril shape induced by deposition on the mica substrate is observed. In addition, fibrils imaged in liquid were completely swollen, while fibrils imaged in air were dried and then left to equilibrate with the environmental humidity. This gives rise to different size and even different compliance of the fibrils. Therefore, due to different adhesion to the substrate and different swelling, AFM measurements yield different fibril diameters in liquid and in air. A similar behaviour is reported in literature. For lithostatine fibrils, Gregoire et al. [28] found a diameter of 7.7 nm obtained by measuring the fibril height in liquid with the AFM. This value is not far from the diameter obtained by the same authors using electron microscopy (~11.7 nm). On the other hand, their AFM measurements in air yield a fibril diameter in the image plane equal to 20–25 nm, broadened, as

expected, by "tip convolution" effects. The fibril height in air is not reported; however, it can be estimated from Eq. (1), taking as R value the nominal radius of curvature of the tips used, which is 10 nm. A lithostatine fibril height between 1 and 2 nm is then obtained, in agreement with our findings on apo A-I.

The fibril diameter resulting from our AFM height measurements in liquid is in agreement with the values provided by different experimental techniques on similar fibrillar systems. In particular, a fibril diameter of $\sim$ 10 nm resulted from electron microscopy analysis of apoA-I (Leu60Arg mutant) fibrils [14,18]. Due to the relatively low adhesion of fibrils to the substrate, limiting the number of observations, and to the lower resolution achieved in liquid, in this case it was not possible to obtain direct information about fibril ultrastructure. Instead, an interesting aspect of images acquired under liquid is the prevalence of globular material, whose role within the process of fibril formation can be manifold. The coexistence of fibrils and globular aggregates in ex vivo samples may be indicative of an equilibrium state, which for apoA-I-LS would include a sizeable fraction of globular aggregates. In this case, globular aggregates would be one intermediate, not necessarily the last one, in the protein misfolding process leading to fibril formation. Alternatively, considering the compatibility of dimensions, globular aggregates may represent building blocks of the protofilaments. In fact, the chromatographic analysis of the sample showed that other fibril components which could form micelles, such as lipids, represented only the 2% w/w of the total. In addition, a simple geometrical model of the fibril structure based on the assembly of protofilaments, whose diameter is equal to the measured globule size, yields a predicted maximum fibril cross section equal to 9.5 ± 0.9, 12 ± 1, and 13 ± 1 nm for three, four and six protofilaments, respectively. While the value obtained for six protofilaments is definitely larger, the values for three and four protofilaments are compatible with the measured fibril size in water, although the errors are too large to allow us to discriminate in favour of either of the latter models. Similar globular structures had been observed previously in other amyloid systems [16,29,30]. The interest in globular precursors has recently increased since in most cases they have been shown to display the highest cytotoxicity whereas mature fibrils appear less toxic or even harmless [29,31,32].

A question which arises is whether the drying procedure used to prepare the sample for measurements in air can induce aggregation of the globular structures into fibrils, thus potentially explaining the discrepancy in the number of fibrils observed in dry and wet samples. However, similar measurements performed on a model system undergoing fibril formation in vitro [33] showed that when only precursors are present, drying of the sample does not alter its morphology. This result suggests that the difference in the number of fibrils observed in liquid and in air may be ascribed to the difficult adhesion of fibrils to mica in the latter case.

Analysis of amyloid fibrils formed by unrelated proteins under different conditions revealed that all fibrils are based on intertwining or juxtaposition of protofilaments whose common internal organization is the cross-β structure. Despite such marked similarity, a variability in morphology and diameter is commonly observed not only for fibrils formed by different peptides, but also for fibrils formed by the same peptide, which often show a polymorphic behaviour [15,29,34]. The ex vivo system analysed in this study displays also heterogeneous morphology, including flat ribbons, cylinders and twisted fibrils. The latter show a left-handed twist, with a helical periodicity of 60–80 nm. The fibril observable features and the geometrical models developed indicate that twisted fibrillar aggregates are formed by three protofilaments. Interestingly, the measured fibril height in air is very similar to that obtained for apoC-II fibrils. It is possible that some of the ribbon structures observed in our sample can simply be based on the stacking of two β-sheets, as proposed for apoC-II [15]. Contrary to that observed for apoC-II and other amyloid systems [15,33], we did not observe ring structures. This may indicate a different fibril flexibility [15]. Alternatively, rings can be intermediate structures which are absent when the aggregation process is completed [33].

These results can be compared with those obtained by Serpell et al. [18], who studied the Leu60Arg apoA-I mutant fibrils by electron microscopy. From the analysis of cross-sectional images, they suggested that fibrils are comprised of five to six protofilaments, approximately 3.2 nm in diameter. However, in the case of the Leu60Arg apoA-I mutant the observed structure was less well resolved compared to other fibrils considered in the same paper. These results could be compatible with those reported here if the protofilaments observed via AFM had themselves a substructure, resulting from the assembly of a pair of thinner protofilaments. Taking into account the resolution of our AFM measurements, this possibility cannot be ruled out.

The availability of amyloid material extracted from two patients affected by hereditary cardiac amyloidosis offered a rare opportunity to compare the aggregation of amyloidogenic apolipoprotein A-I in vivo in two unrelated cases. An interesting feature of the material examined is the coexistence of fibrils and globular aggregates. The latter, on the basis of the present study, are proposed to act as fibril precursors. As a result of continuous production of amyloidogenic protein by the body, different steps of the aggregation process are then proposed to be present at the same time. In fact, confirming that fibril formation was still in progress, some years after heart transplantation both patients became again affected by the disease.

Our AFM measurements show that not only mature fibrils, which are the final product of the aggregation, but also pre-fibrillar aggregates display in both cases examined the same structural features, with common morphologies and compatible sizes of fibrils and globules. This result has important implications since it suggests that fibril formation

occurs according to a well-defined aggregation pathway, which seems to be essentially unaffected by peculiar features of each patient.

Acknowledgements

The authors thank Dr. Claudio Canale for helping with AFM measurements and data elaboration. This work was partially supported by MIUR (projects FIRB RBNE01S29H and RBAU015B47, PRIN 2002058218 and 2003051399), by CNR (project ''Genetica Molecolare''), by Telethon (project number 164-11477) and by Ministero della Sanità (ricerca finalizzata Malattia di Alzheimer).

References

[1] C.M. Dobson, Protein folding and its links with human disease, Biochem. Soc. Symp. 68 (2001) 1–26.
[2] M. Bucciantini, E. Giannoni, F. Chiti, F. Baroni, L. Formigli, J. Zurdo, N. Taddei, G. Ramponi, C.M. Dobson, M. Stefani, Inherent toxicity of aggregates implies a common mechanism for protein misfolding diseases, Nature 416 (2002) 507–511.
[3] J.W. Kelly, Mechanisms of amyloidogenesis, Nat. Struct. Biol. 7 (2000) 824–826.
[4] L.O. Tjernberg, D.J. Callaway, A. Tjernberg, S. Hahne, C. Lilliehook, L. Terenius, J. Thyberg, C. Nordstedt, A molecular model of Alzheimer amyloid beta-peptide fibril formation, J. Biol. Chem. 274 (1999) 12619–12625.
[5] O.N. Antzuktin, R.D. Leapman, J.J. Balbach, R. Tycko, Supramolecular structural constraints on Alzheimer's beta-amyloid fibrils from electron microscopy and solid-state nuclear magnetic resonance, Biochemistry 41 (2002) 15436–15450.
[6] H.H. Bauer, U. Aebi, M. Häner, R. Hermann, M. Müller, T. Arvinte, H.P. Merkle, Architecture and polymorphism of fibrillar supramolecular assemblies produced by in vitro aggregation of human calcitonin, J. Struct. Biol. 115 (1995) 1–15.
[7] D.A. Kirschner, R. Elliott-Bryant, K.E. Szumowski, W.A. Gonnerman, M.S. Kindy, J.D. Sipe, E.S. Cathcart, In vitro amyloid fibril formation by synthetic peptides corresponding to amino terminus of apoSAA isoforms from amyloid-susceptible and amyloid-resistant mice, J. Struct. Biol. 124 (1998) 88–98.
[8] C. Goldsbury, K. Goldie, J. Pellaud, J. Seelig, P. Frey, S.A. Muller, J. Cooper, G.J. Cooper, U. Aebi, Amyloid fibril formation from full-length and fragments of amylin, J. Struct. Biol. 130 (2000) 352–362.
[9] H. Inouye, D.A. Kirschner, X-ray diffraction analysis of scrapie prion: intermediate and folded structures in a peptide containing two putative alpha-helices, J. Mol. Biol. 268 (1997) 375–389.
[10] J.L. Jiménez, J.I. Guijarro, E. Orlova, J. Zurdo, C.M. Dobson, M. Sunde, H.R. Saibil, Cryo-electron microscopy structure of an SH3 amyloid fibril and model of the molecular packing, EMBO J. 18 (1999) 815–821.
[11] C. Ionescu-Zanetti, R. Khurana, J.R. Gillespie, J.S. Petrick, L.C. Trabachino, L.J. Minert, S.A. Carter, A.L. Fink, Monitoring the assembly of Ig light-chain amyloid fibrils by atomic force microscopy, Proc. Natl. Acad. Sci. U. S. A. 96 (1999) 13175–13179.
[12] N.M. Kad, S.L. Myers, D.P. Smith, D.A. Smith, S.E. Radford, N.H. Thomson, Hierarchical assembly of β_2-microglobulin amyloid in vitro revealed by atomic force microscopy, J. Mol. Biol. 330 (2003) 785–797.
[13] I. Cardoso, C.S. Goldsbury, S.A. Muller, V. Olivieri, S. Wirtz, A. Damas, U. Aebi, M.J. Saraiva, Transthyretin fibrillogenesis entails the assembly of monomers: a molecular model for in vitro assembled transthyretin amyloid-like fibrils, J. Mol. Biol. 317 (2002) 683–695.
[14] J.L. Jimenez, G. Tennent, M. Pepys, H.R. Saibil, Structural diversity of ex vivo amyloid fibrils studied by cryo-electron microscopy, J. Mol. Biol. 311 (2001) 241–247.
[15] D.M. Hatters, C.A. MacRaild, R. Daniels, W.S. Gosal, N.H. Thomson, J.A. Jones, J.J. Davis, C.E. MacPhee, C.M. Dobson, G.J. Howlett, The circularization of amyloid fibrils formed by apolipoprotein C-II, Biophys. J. 85 (2003) 3979–3990.
[16] A.K. Chamberlain, C.E. MacPhee, J. Zurdo, L. Morozova-Roche, H.A.O. Hill, C.M. Dobson, J.J. Davis, Ultrastructural organization of amyloid fibrils by atomic force microscopy, Biophys. J. 79 (2000) 3282–3293.
[17] P. Mangione, M. Sunde, S. Giorgetti, M. Stoppini, G. Esposito, L. Gianelli, L. Obici, L. Asti, A. Andreola, P. Viglino, G. Merlini, V. Bellotti, Amyloid fibrils derived from the apolipoprotein A-I Leu174Ser variant contain elements of ordered helical structure, Protein Sci. 10 (2001) 187–199.
[18] L.C. Serpell, M. Sunde, M.D. Benson, G.A. Tennent, M.B. Pepys, P.E. Fraser, The protofilament substructure of amyloid fibrils, J. Mol. Biol. 300 (2000) 1033–1039.
[19] L. Obici, V. Bellotti, P. Mangione, M. Stoppini, E. Arbustini, L. Verga, I. Zorzoli, E. Anesi, G. Zanotti, C. Campana, M. Vigano, G. Merlini, The new apolipoprotein A-I variant $Leu^{174} \rightarrow Ser$ causes hereditary cardiac amyloidosis, and the amyloid fibrils are constituted by the 93-residue N-terminal polypeptide, Am. J. Pathol. 155 (1999) 695–702.
[20] M. Pras, D. Schubert, D. Zucker-Franklin, A. Rimon, A.C. Franklin, The characterization of soluble amyloid prepared in water, J. Clin. Invest. 47 (1968) 924–933.
[21] H. LeVine, Quantification of β-sheet amyloid fibril structure Method, Enzymology 309 (1999) 274–284.
[22] A. Andreola, V. Bellotti, S. Giorgetti, P. Mangione, L. Obici, M. Stoppini, J. Torres, E. Monzani, G. Merlini, M. Sunde, Conformational switching and fibrillogenesis in amyloidogenic fragment of apolipoprotein A-I, J. Biol. Chem. 278 (2003) 2444–2451.
[23] B.A. Watkins, S.L. Feng, A.K. Strom, A.A. DeVitt, L. Yu, Y. Li, Conjugated linoleic acids alter the fatty acid composition and physical properties of egg yolk and albumen, J. Agric. Food Chem. 51 (2003) 6870–6876.
[24] K.A. Ramirez-Aguilar, K.L. Rowlen, Tip characterization from AFM images of nanometric spherical particles, Langmuir 14 (1998) 2562–2566.
[25] M.F. Perutz, J.T. Finch, J. Berriman, A. Lesk, Amyloid fibers are water filled nanotubes, Proc. Natl. Acad. Sci. U. S. A. 99 (2002) 5591–5595.
[26] R. Raiteri, S. Martinoia, M. Grattarola, pH dependent charge density at the insulator-electrolyte interface probed by a scanning probe microscope, Biosens. Bioelectron. 11 (1996) 1009–1017.
[27] D.J. Müller, A. Engel, The height of biomolecules measured with the atomic force microscope depends on electrostatic interactions, Biophys. J. 73 (1997) 1633–1644.
[28] C. Grégoire, S. Marco, J. Thimonier, L. Duplan, E. Laurine, J.-P. Chauvin, B. Michel, V. Peyrot, J.-M. Verdier, Three-dimensional structure of lithostathine protofibril, a protein involved in Alzheimer's disease, EMBO J. 20 (2001) 3313–3321.
[29] M. Stefani, C.M. Dobson, Protein aggregation and aggregate toxicity: new insights into protein folding, misfolding diseases and biological evolution, J. Mol. Med. 81 (2003) 678–699.
[30] J.D. Harper, S.S. Wong, C.M. Lieber, P.T. Lansbury, Assembly of Aβ amyloid protofibrils: an in vitro model for a possible early event in Alzheimer's disease, Biochemistry 38 (1999) 8972–8980.
[31] M. Hoshi, M. Sato, S. Matsumoto, A. Noguchi, K. Yasutake, N. Yoshida, K. Sato, Spherical aggregates of β-amyloid (amylospheroid) show high neurotoxicity and activate tau protein kinase I/glycogen synthase kinase-3β, Proc. Natl. Acad. Sci. U. S. A. 100 (2003) 6370–6375.

[32] R. Kayed, E. Head, J.L. Thompson, T.M. McIntire, S.C. Milton, C.W. Cotman, C.G. Glabe, Common structure of soluble amyloid oligomers implies common mechanisms of pathogenesis, Science 300 (2003) 486–489.
[33] A. Relini, C. Canale, S. Torrassa, R. Rolandi, A. Gliozzi, C. Rosano, M. Bolognesi, G. Plakoutsi, M. Bucciantini, F. Chiti, M. Stefani, Monitoring the process of HypF fibrillization and liposome permeabilization by protofibrils, J. Mol. Biol. 338 (2004) 943–957.
[34] O.N. Antzutkin, Amyloidosis of Alzheimer's A beta peptides: solid-state nuclear magnetic resonance, transmission electron microscopy, scanning trasmission electron microscopy and atomic force microscopy studies, Magn. Reson. Chem. 42 (2004) 231–246.